Journal of The Electrochemical Society, **166** (2) C65-C75 (2019)
0013-4651/2019/166(2)/C65/11/$37.00 © The Electrochemical Society

The Contrast between the Pitting Corrosion of 316 SS in NaCl and NaBr Solutions: Part I. Evolution of Metastable Pitting and Stable Pitting

S. Pahlavan, M. H. Moayed, [z] and M. Mirjalili

Department of Materials and Metallurgical Engineering, Faculty of Engineering, Ferdowsi University of Mashhad, Mashhad 91775-1111, Iran

This paper contrasts metastable and stable pitting of 316 austenitic stainless steel in chloride and bromide bearing solutions. Metastable and stable pitting characteristics were evaluated by potentiostatic and potentiodynamic polarization experiments, respectively. Results revealed that for a given concentration of halide anions, pitting and repassivation potentials rise by increasing the Br^-:Cl^- concentration ratio in the environment. Increasing the relative concentration of Br^- also leads to a decrease in the values of metastable pit stability product. Furthermore, higher concentration of bromide in the solution reduces the growth kinetics of metastable pits. Using pencil electrodes, it was also found that hindrance of the dissolution reactions in presence of bromide anion could be responsible for the lower aggressivity of bromide and the observed decrement in metastable growth kinetics.
 [DOI: 10.1149/2.0811902jes]

Manuscript submitted October 22, 2018; revised manuscript received January 14, 2019. Published January 24, 2019.

Nobody can disclaim the importance of stainless steels (SSs) in today's world. Their importance is due to their capability to form an adherent passive film which impedes the substrate corrosion. The cause of passive film formation is the existence of at least 11% Cr in the SSs composition.[1,2] Formed passive films on SSs are not entirely perfect and some species known as aggressive anions can develop localized breakdown events on their weak points such as grain boundaries, dislocations, and inclusions. A localized breakdown event can lead to the accelerated dissolution of the alloy inside an occluded region called a pit and hence, cause pitting corrosion to ensue.[2–5] After pit nucleation by passivity breakdown, the pitting process usually consists of two stages of metastable and stable growth.[4,6–10] Each nucleation event is usually followed by a state of metastable growth during which a lacy cover forms on the pit mouth.[11–17] At early stages of pit growth, this lacy cover provides the adequate diffusion barrier required for maintenance of the aggressive environment within the pit which is able to hamper the repassivation, thermodynamically. Successive partial ruptures of the lacy cover during the metastability lead to stepwise increases in the current triggered by the alloy dissolution. If the lacy cover completely ruptures during the metastable growth, the pit will die.[11,14,18]

The study of metastable pits has been always of great interest regarding investigation of pitting. This matter stems from the inseparability of stable and metastable pitting. As reported, they can be observed as transient fluctuations of potential under open-circuit condition or galvanostatic control, or of current under potentiostatic control.[4,7,19,20] What is more, they also appear as current fluctuations in potentiodynamic polarizations below the pitting potential (above the critical pitting temperature, *CPT*).[21–23] Apart from this habitual presence, there are correspondences between the features of metastable pits and those of stable ones making their study more intriguing.[4,19,20,24,25] For instance, early growth of them has been reported to be identical. Indeed, all pits whether repassivate at the metastable stage or keep growing to become stable, are initiated as metastable pits.[21,26] The formation rate of stable pits is also believed to be a function of that of metastable pits and their probability for becoming stable.[19] Therefore, any change in metastable pitting features is likely to correlate with stable pitting, as well.

The stability product is a criterion proposed by Galvele and it is defined as the product of pit depth, a, and its current density, i. For the transition of a pit from metastability to stability, the pit's stability product must exceed a critical value which corresponds with the critical pit environment needed for passivation not to ensue. In such a case, the pit depth is sufficient by itself for retention of the critical pit solution.[6,7,14,27,28] It is hence obvious that every stable pit begins to develop by metastable growth, initially. By progressive alloy dissolution in the process of pitting, the pit solution becomes enriched in metal cations. The metal cations can bond with aggressive anions and form a salt (predominantly hydrated $FeCl_2$)[29] which will be able to precipitate within the pit and establish diffusion-controlled growth.[4,6,7,11,16,26,30,31] Besides, an already stable pit can remain active even down to a potential lower than E_{pit}, which is called repassivation potential, E_{rep}, due to retaining of the critical environment within the pit.[7]

Amongst the numerous reported aggressive anions, chloride and bromide are of a great importance because they can induce pitting for a lot of alloys such as SSs, aluminum, nickel, titanium, zirconium and zinc.[3] It has been frequently reported that the aggressivity of halides decreases in the order of: $Cl^- > Br^- > I^-$.[32–37] Notwithstanding the foregoing reports, many researchers have observed that for SSs with higher content of Mo, Br^- shows more aggressivity than Cl^-.[38,39] Fewer metastable pits formed in bromide bearing solutions than in chloride bearing ones and their characteristics such as peak current, radius and stability product were lower, accordingly.[35,37]

The largest family of SSs, in terms of multiplicity and applications are the austenitic ones. Their main alloying element is Ni which stabilizes the austenite and enhances the corrosion resistance. 316 SS is a popular member of the austenitic family and can resist the corrosive attack of chemicals used in production of ink, rayon, paper, textiles, rubber, bleaches and photographic chemicals. It is also usable in some surgical implants.[1,2]

This work aims to contrast the pitting behavior of 316 SS in NaCl and NaBr solutions and give in-depth information about the metastable and stable pitting in these media. Evaluation of the E_{pit} and E_{rep} can divulge the alloy susceptibility to the pitting corrosion in different environments. The study of metastable pitting is also able to provide valuable information about the kinetics of pit growth as it has been highlighted by researchers, repeatedly.[6,8,11,25,40–42] In the second part of the paper, pit chemistry characteristics is studied using pencil electrode to further discover the reason of the difference in the aggressivity of chloride and bromide anions. The morphology of the pits is also examined using scanning electron microscope.

Experimental

Materials and preparations.—The studied material in this work was a solution-annealed cylindrical alloy of 316 SS which its chemical composition has been listed in Table I. The alloy was cut in two sizes: 0.785 cm^2 × 1 cm and 0.071 cm^2 × 1 cm (surface × height). The smaller exposed surface was used for metastable pitting investigation and the bigger one for stable pitting. In order to eliminate the risk of crevice corrosion occurrence in the alloy/mount interface, the specimens were primarily prepassivated in 0.1 M Na_2SO_4 solution.[9,35,43] Prepassivation was implemented by polarising the specimens at 850 mV_{SCE}, for 0.5 h. Specimens were then mounted in an inert epoxy

[z]E-mail: mhmoayed@um.ac.ir

Table I. The chemical compositions of the 316 stainless steels used in this study.

Alloy	Fe	Cr	Ni	Mo	Mn	Si	C	P	S
Cylindrical 316 SS (1 cm dia.)	Bal.	18.1	10.5	2.10	1.9	0.4	0.050	0.020	0.012
Wire of 316 SS (50 μm dia.)	Bal.	18.7	10.8	2.05	2.1	0.5	0.045	0.019	0.015

resin and their connections were established by means of a screw and a copper wire. Prior to each test, surfaces of these flat electrodes were wet-ground up to 1200 SiC paper, washed by distilled water and dried with flowing warm air.

Some experiments were also performed on a wire of 316 SS (diameter of 50 μm) as pencil electrodes (surface area = 1.963×10^{-5} cm^2). The chemical composition of this material has been also included in Table I. Pencil electrodes were similarly mounted in an inert epoxy resin and the electrical connections were established by means of a copper wire. Prior to each experiment using these electrodes, they were wet-ground by 60 SiC paper, rinsed by distilled water and dried with flowing warm air.

Potentiodynamic experiments.—Potentiodynamic (PD) experiments were used for evaluation of the stable pitting characteristics. The conventional three-electrode technique was used for this purpose. A saturated calomel electrode (SCE), a platinum plate and 316 SS specimens were served as reference, auxiliary and working electrodes, respectively. Open circuit potential (OCP) was firstly recorded for 0.5 h in all experiments to obtain the steady state condition. The polarization was then begun from −50 mV respect to the OCP, up to the pitting onset by the sweep rate of 1 $mV \cdot s^{-1}$. Additionally, to determine the repassivation potential, the sweep was reversed at the rate of -1 $mV \cdot s^{-1}$ after the current density reached the value of 0.1 $mA \cdot cm^{-2}$. Experiments were carried out at the ambient temperature (21±3°C) and repeated 15 times for each solution to check data reproducibility.

PD experiments were conducted in different concentrations of chloride and bromide bearing solutions. The solutions were prepared using reagent grade chemicals and distilled water. The cell was also a 250 ml beaker open to the air.

Potentiostatic experiments.—For statistical study of the metastable pitting of 316 SS in chloride and bromide bearing solutions, potentiostatic (PS) experiments were utilized. A potential in the range of passivity, i.e. 100 mV_{SCE}, was applied to 316 SS electrodes and the current was recorded for 1200 s. To obtain the steady state condition, the OCP was measured for 0.5 h before running the PS polarization. Data acquisition rate was also set to 45 Hz. Experiments were carried out at the ambient temperature (21±3°C) and repeated thrice to check data reproducibility and to survey the metastable pits more accurately. Investigated solutions were: 0.2 M NaCl, 0.15 M NaCl + 0.05 M NaBr, 0.1 M NaCl + 0.1 M NaBr, 0.05 M NaCl + 0.15 M NaBr and 0.2 M NaBr solutions. The electrochemical cell in this case was also a 250 beaker open to the air.

Pencil electrode studies.—A kind of PD experiments was performed in order to assess the effect of bromide on the rate of alloy dissolution within a pit before salt precipitation. The aim of these experiments is to discover the rationale of possible differences in metastable pit growth rates. In these tests, 316 SS pencil electrodes were polarized from −50 mV respect to the OCP up to anodic potentials with the sweep rate of 10 $mV \cdot s^{-1}$; pencil electrodes were places upward in the test solution. The studied solutions in these tests were simulated pit solutions: 5 M HCl + 1 M NaCl and 5 M HBr + 1 M NaBr. The cell in these test was also a 250 ml beaker open to the air.

In order to compare the rate of alloy dissolution in actual pitting conditions, the pencil electrodes of 316 SS were first potentiostatically polarized at 850 mV_{SCE} for 900 s to develop stable artificial pits. The potential was then dropped to 350 mV_{SCE}. The polarization at this potential also proceeded for 900 s to reach a stable condition of pit growth under the diffusion controlled regime (salt stabilization). Afterwards, the potential was reduced at the rate of -1 $mV \cdot s^{-1}$ down until the complete dissolution of the salt and appearance of the active/ohmic controlled regime.[30,44] Investigated solutions were pure 0.2 M solutions of NaCl and NaBr. The electrochemical cell in this case was similarly a 250 beaker open to the air.

Results

Stable pitting characteristics.—Figure 1 compares the PD behavior of 316 SS in combined NaCl and NaBr solutions. In order to avoid any possible complexity, upward and reverse scans have been

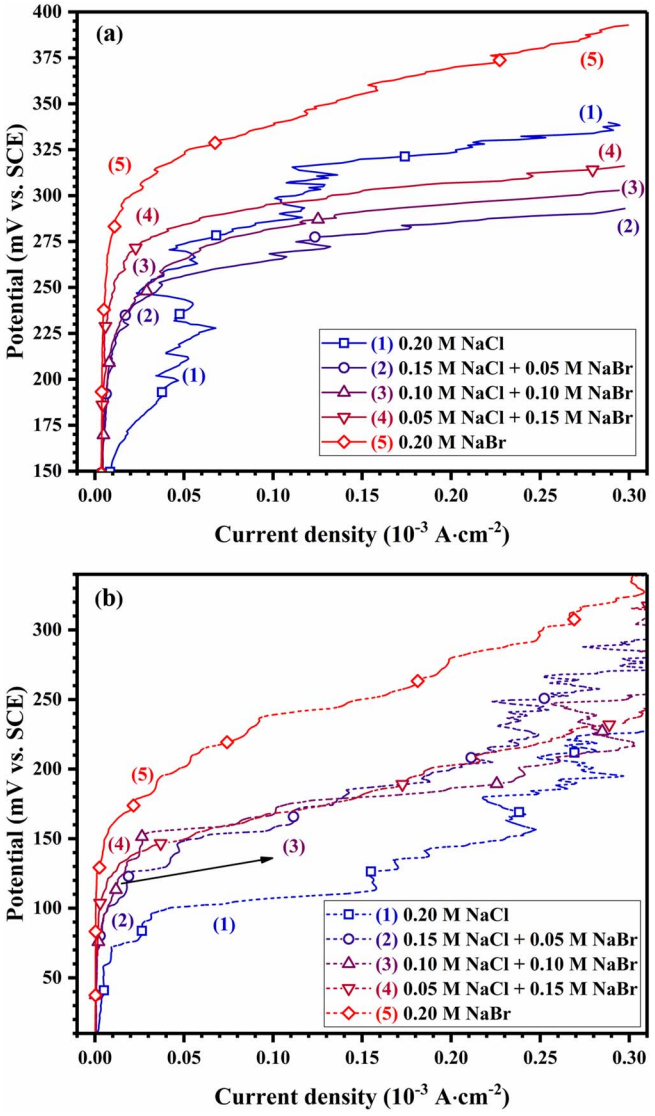

Figure 1. Typical PD curves obtained in combined NaCl and NaBr solutions. a) Upward sweeps for determination of E_{pit} (solid lines). b) Corresponding downward sweeps for determination of E_{rep} (dashed lines). Sweep rate: 1 $mV \cdot s^{-1}$. Electrode surface area: 0.785 cm^2.

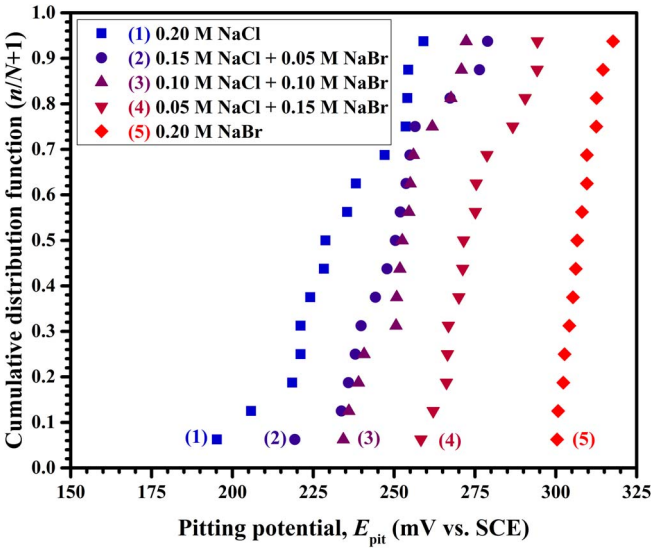

Figure 2. Cumulative distribution of the pitting potential, E_{pit}, for combined NaCl and NaBr solutions.

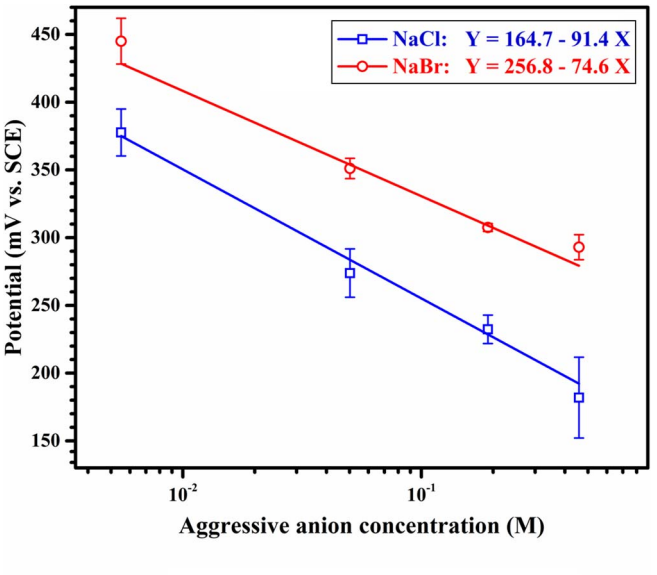

Figure 3. Pitting potential, E_{pit}, of 316 SS as a function of log C_{agg} in pure NaCl and pure NaBr solutions. C_{agg}, denotes the concentration of the aggressive anion. Error bars are also indicating the 95% confidence limit obtained from 15 identical experiments.

represented, separately. As can be seen, 316 SS is susceptible to pitting corrosion in all these solutions. Besides, the increment of pitting and repassivation potentials by increasing the relative concentration of Br^- is clearly observable in the figure. Another fact is the smoother breakdown of the polarization curve in Br^- bearing solutions in comparison with the Cl^- bearing ones. In other words, successive decrements and increments of current density in bromide bearing solutions are much lower than those compared to the pure chloride bearing one.

Pitting Potential, E_{pit}.—Since pitting corrosion is an unpredictable and stochastic phenomenon, the pitting potential cannot be considered as a unique value.[9,22,45,46] Hence, repeated experiments are needed for correct determination of the pitting potential, E_{pit}. Cumulative distributions of E_{pit}, in the combined NaCl and NaBr solutions have been shown in Figure 2. E_{pit} in this work was considered as the potential at which current density increased suddenly without reversion.[35] The horizontal axis in Figure 2 is E_{pit} and the vertical one is the cumulative probability which can be calculated by using Equation 1:[46,47]

$$P(E) = \frac{n}{1+N} \quad [1]$$

where N is the total number of events (measurements) and n is the number of each event. In order to compare E_{pit} in different solutions, the median values of them, $P(E) = 0.5$, can be used. Based on Figure 2, it can be said that a higher concentration of bromide in the environment causes the E_{pit} to increase. Therefore, the lowest and highest pitting potentials were obtained in pure 0.2 M NaCl and 0.2 M NaBr solutions, respectively.

In this study E_{pit}, was measured for different concentrations of pure NaCl and pure NaBr solutions too. The measurements were repeated 15 times for each solution and the average values of E_{pit} have been represented in Figure 3. As can be seen, by decreasing the concentration of each anion, the pitting potential increases. Furthermore, it is evident that the value of E_{pit} for a constant concentration of halide anion is lower for NaCl solution. Figure 3 also shows that there is a linear relationship between E_{pit} and logarithm of aggressive anion concentration, C_{agg}, The existence of this linear relationship has been repeatedly reported in published literature.[3,7,27,35,48,49] Equation 2 describes this relationship, as follows:

$$E_{pit} = A - B \log C_{agg} \quad [2]$$

A and B are constants which differ for different systems.

The line slopes for NaCl and NaBr solutions have been calculated to be about 91.4 and 74.6 mV · decade^{-1}, respectively. The line slope for NaCl solutions has been reported to vary between 50–100 mV · decade^{-1}.[49] It must be noted that in a similar work, the line slopes for 403 SS in NaCl and NaBr solution have been approximately obtained as 131 and 80 mV · decade^{-1}.[35] As seen in Figure 3, the values of constant A for NaCl and NaBr solutions are about 165 and 257 mV, respectively. According to Equation 2, A is an estimation of the pitting potential, E_{pit}, in the 1 M solution of aggressive anion.

Repassivation Potential, E_{rep}.—Figure 4 compares repassivation potentials of flat electrodes, E_{rep}, for different combined NaCl and NaBr solutions. Pure 0.2 M NaCl and 0.2 M NaBr solutions have the lowest and highest repassivation potentials, respectively. The repassivation potentials for combined solutions also have values between the foregoing two.

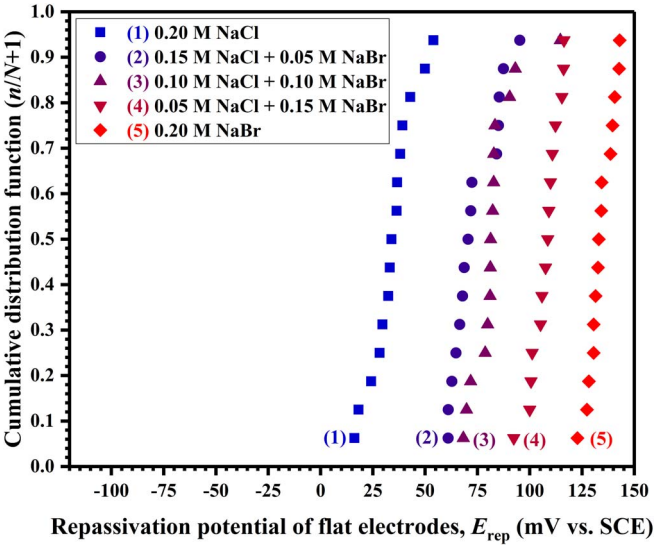

Figure 4. Cumulative distribution of the repassivation potential, E_{rep}, for combined NaCl and NaBr solutions.

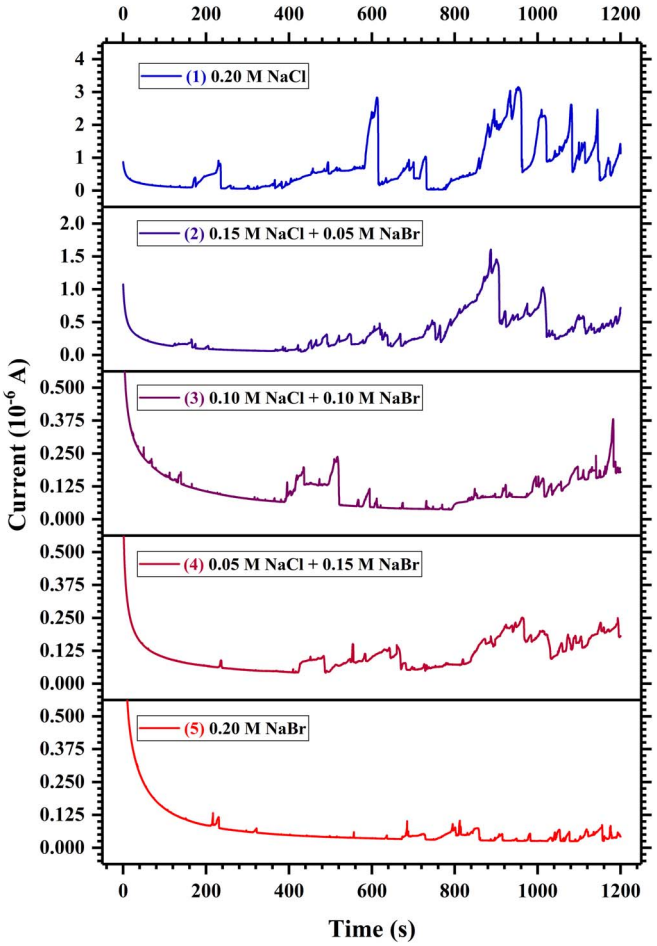

Figure 5. Typical current-time behavior of the 316 SS electrode, at 100 mV_{SCE}, in combined NaCl and NaBr solutions. Electrode surface area: 0.071 cm^2. Data acquisition rate: 45 Hz.

The fact that by increasing the relative concentration of Br^- in combined NaCl and NaBr solutions, E_{rep} will possess more noble values (Figure 4), implies that in bromide bearing environments, the growth of a stable pit could cease at higher potentials. That is, survival of a stable pit at low potentials is of higher difficulty when the solution bears bromide. In other words, the critical pit solution which is required for survival of already stabilized pits on 316 SS could be missed sooner in bromide bearing solutions compared to chloride bearing ones. According to previous reports, some steels have had lower E_{rep} in bromide bearing solutions, though.[33]

Statistical characteristics of metastable pits.—Typical PS curves obtained for 316 SS in combined NaCl and NaBr solutions at 100 mV_{SCE} are represented in Figure 5. As can be seen, by putting the 316 SS flat electrodes at this potential, the recorded current begins to decrease to a relatively constant baseline value due to the formation of the passive film. The existing fluctuations on the current curve are referred to as the metastable pitting events. Considering Figure 5, it can be said that the pitting corrosion of 316 SS in all combined solutions of NaCl and NaBr is associated with the metastable pitting events.

The feature of the metastable pits for all studied solutions including pure NaBr one, as can be seen, is akin to those which have been already reported for SSs, having a gradual growth and a sudden repassivation.[6,7,11,26,50] As it is obvious in Figure 5, although in these tests the electrode surface was smaller (0.071 cm^2) in comparison with the specimens used in PD experiments (0.785 cm^2), there are still some overlapping transients on the curve of all solutions. It was reported that secondary and multiple pit nucleation occur

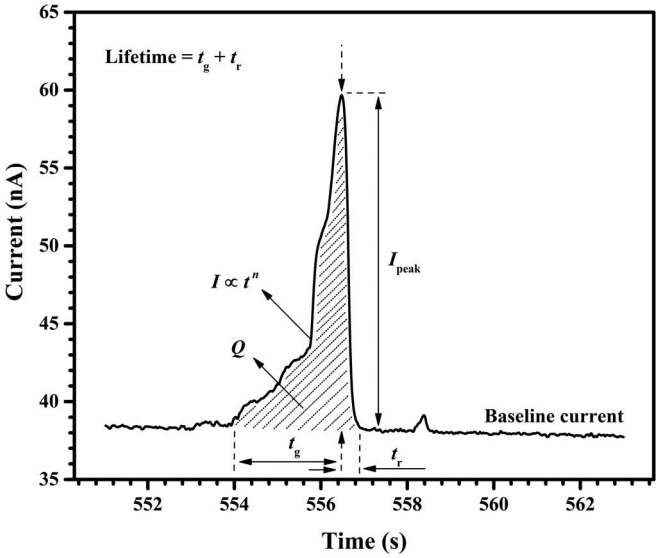

Figure 6. A typical metastable pit with some of its corresponding definable quantities: lifetime, growth time, repassivation time, peak current, dissolved charge and baseline current.

if sulfur-containing compounds or other readily dissolved metallographic defects are exposed during the metastable growth of a pit, causing overlapping current transients to be produced.[50] Comparing the PS curves in Figure 5, it can be said that large current transients in pure NaCl solution vastly outnumber these transients in pure NaBr solution. The same observations have been reported for 403[35] and Fe-13Cr[37] martensitic SSs. Due to the high baseline current at the primary stages of the PS experiments, the first 200-second period was ignored and the next 1000-second period was used for statistical analysis of the metastable pitting. Therefore, coming figures do not comprise the current transients appearing before the 200th second of the PS experiments.

Figure 6 illustrates a typical metastable pit that appeared on 316 SS in 0.05 M NaCl + 0.15 M NaBr solution. It is believed that there is an exponential relationship between the current, I, and time, t, for a metastably growing pit, as shown in the figure: $I \sim t^n$[7,11,17,26,51,52] Furthermore, for each individual metastable pit like the one indicated in Figure 6, various quantities can be defined and compared under different circumstances.[8,22,35,42,53] Some of these quantities are introduced, as follows:

- Lifetime: the difference between the nucleation and the repassivation points which is equal to the summation of the growth time, t_g, and the repassivation time, t_r (shown in Figure 6).
- Peak current, I_{peak}: the highest current recorded during the lifetime of a given metastable pit.
- Radius, a: the radius of a hemisphere which is assumed to be created by each metastable pitting event. The radius is calculated by integrating the current curve over the metastable pit growth time and by applying the Faraday's law,[8,9,22,35,45] in accordance with Equation 3. Z and ρ in this equation are respectively mean molar mass and mean density of the alloy which can be calculated using the mole fractions of Fe, Cr and Ni. n is also the mean oxidation state of cations. F and I are Faraday's constant (96485 $C \cdot mol^{-1}$) and current, respectively. For the cylindrical 316 SS alloy used in this study, Z is 55.36 $gr \cdot mol^{-1}$, ρ is 7.84 $gr \cdot cm^{-3}$, and n is 2.202.

$$a = \left(\frac{3Z\int I dt}{2\pi n F \rho}\right)^{\frac{1}{3}} \quad [3]$$

- Current density, i: metastable pit current density could be calculated by dividing the current, I, by the surface area of the hemisphere-assumed metastable pit, $2\pi a$.[2 11,35]
- Stability product, $i \cdot a$: the product of metastable pit current density, i, and its radius, a. According to Galvele,[6,27,28] the requirement for transition of a pit from metastability to stability is that its stability product exceeds a certain critical value.

Peak current.—The cumulative distribution of metastable peak current, I_{peak}, has been plotted in Figure 7a. As can be seen, the highest median value of I_{peak} which belongs to the pure 0.2 M NaCl solution, is almost 1 decade more than the lowest one which was obtained for pure 0.2 M NaBr one. The values for combined solutions are situated between them, virtually. Ignoring some aberrations seen in the figure, it can be said that I_{peak} decreases by increment of the relative concentration of the Br^- in the studied solutions.

Radius.—Figure 7b depicts the cumulative distribution of metastable pit radius for different combined chloride and bromide bearing solutions. Note that these values are corresponding to the peak points, the currents of which have been shown in Figure 7a. For a certain concentration of the halide anion (Cl^- or Br^-), the largest sizes of the pits have been developed in pure NaCl solution, with the median value of about 1 μm. Increasing the relative concentration of Br^- in the solution caused the pits to possess smaller radii. It is however evident in Figure 7b, that the solutions 3, 4 and 5 (note the concentrations in the figure) have a very similar distribution in terms of the metastable pit radii, so that they are not distinguishable in the figure, easily.

Stability product.—The calculated metastable stability product at the peak point for different combined NaCl and NaBr solutions have been represented in Figure 7c, in the form of cumulative distribution function. The increment of the stability product value by increasing the Cl^-:Br^- concentration ratio, is perceptible in the figure. As a quantitative statement, the median value of metastable stability product for pure solutions of NaCl is almost 6.2 $mA \cdot m^{-1}$ more than that for pure 0.2 M solution of NaBr.

Table II lists the median values of metastable pits peak current, radius, and stability product.

Occurrence frequency of metastable Pits, **λ.—**Figure 8 compares the occurrence frequency of metastable pits, λ, for different chloride and bromide bearing solutions. Occurrence frequency, λ, was defined as the total number of initiated metastable pits on a unit area, in each 100-second interval.[8,9,22,35,45,52] As an example, by dividing the total number of metastable pits between the 400th and 500th seconds of a PS experiment, by 100 and by the electrode exposed surface, λ can be obtained for the point 450 s on the time axis.

Considering the Figure 8, no remarkable difference is established in occurrence frequency by increasing the relative concentration of Br^- in the solutions. This is while in an earlier study, metastable pits occurrence frequency of 403 SS in NaBr solutions was noticeably lower in comparison with the NaCl solution.[35]

The falling trend of occurrence frequency over the time is, however, roughly recognizable in the figure. As alluded to in previous studies, occurrence frequency of metastable pits decreases with exposure time, exponentially. The falling trend of λ is attributed to diminishing of the preferential sites for pit nucleation over the time, due to multiple nucleation and repassivation of metastable pits on the surface.[8,9,35,45]

Growth kinetics of metastable pits.—The value of n in $I \sim t^n$ behavior of the metastable pits is an indicative of their growth kinetics. To determine this value, a simple linear relationship (Equation 4) could be fitted to the $\log I \sim \log t$ curve of individual metastable pits.[7,26,51,52] Since the metastable pit radius is a function of its current (Equation 3), a similar relationship could be written between radius and time, as well (Equations 5). In Equations 4 and 5, k_I, n_I, k_a, and n_a are all

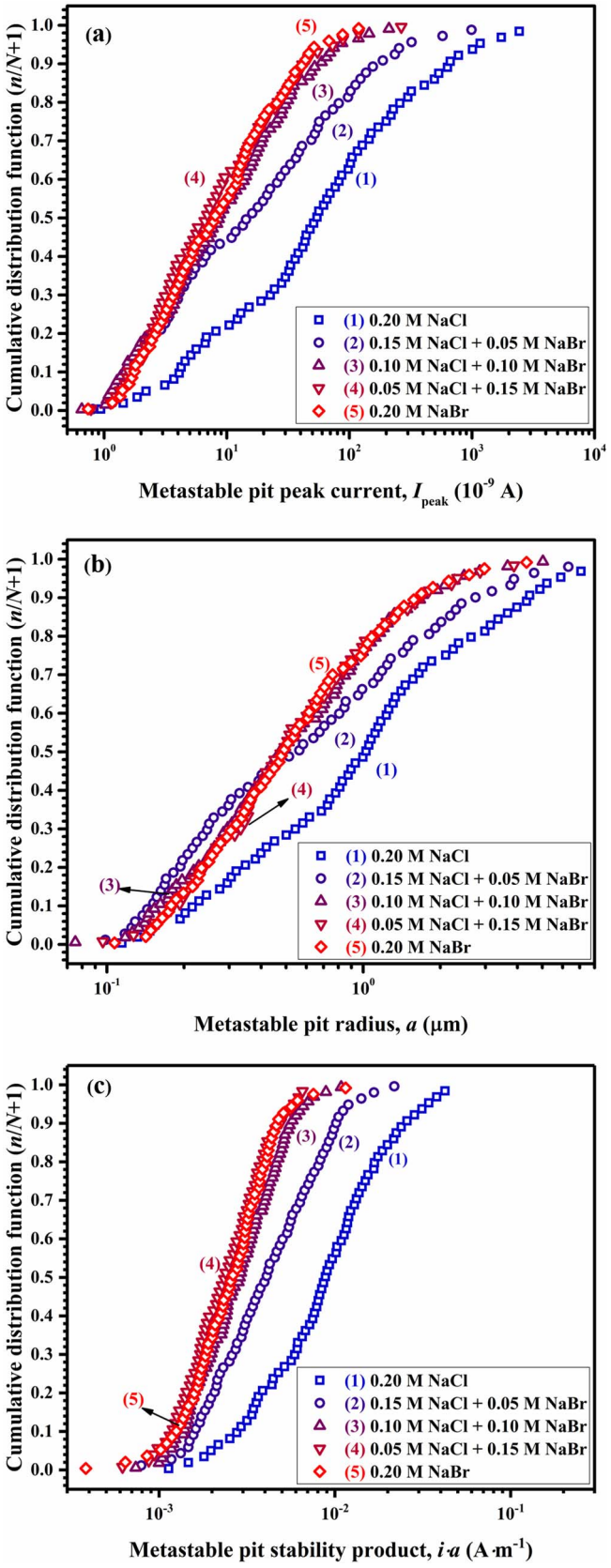

Figure 7. Cumulative distribution of a) lifetime, b) radius, and c) stability product of metastable pits in combined NaCl and NaBr solutions.

Table II. Median values for metastable pits peak current, radius, and stability product in NaCl + NaBr solutions.

Solution	0.20 M NaCl	0.15 M NaCl + 0.05 M NaBr	0.10 M NaCl + 0.10 M NaBr	0.05 M NaCl + 0.15 M NaBr	0.20 M NaBr
Peak current (nA)	54.43	14.52	8.68	6.76	7.94
Radius (μm)	1.026	0.548	0.473	0.483	0.489
Stability Product ($mA \cdot m^{-1}$)	8.834	4.065	2.869	2.355	2.629

constants, varying for different systems.

$$\log I = k_I + n_I \log t \quad [4]$$

$$\log a = k_a + n_a \log t \quad [5]$$

Assessment of the kinetic parameters shown in Equations 6 and 7 (i.e. n_I and n_a) for the metastable pits that appeared in PS polarization curves (Figure 5) could assist in comparing the growth kinetics of metastable pits for NaCl and NaBr solutions. To assess these parameters, in a reliable way, it was firstly decided to categorize the metastable pits into three groups: small, moderate, and large metastable pits. Small metastable pits were those whose peak current in Figure 7a was close to $I_{0.25}$ and $P(I_{0.25}) = 0.25$. Moderate and large metastable pits were also those whose peak currents were respectively comparable to $I_{0.5}$ and $I_{0.75}$, bearing in mind that $P(I_{0.5}) = 0.5$ and $P(I_{0.75}) = 0.75$. According to the values of peak current shown in Figure 7a, $I_{0.25}$, $I_{0.5}$, and $I_{0.75}$ for 0.2 M solution of NaBr are respectively 3.1, 7.9, and 19.2 nA. For 0.2 M solution of NaCl also, $I_{0.25}$, $I_{0.5}$, and $I_{0.75}$ are 12.5, 54.2, and 195.3 nA, respectively. From each group, 5 distinct metastable pits were randomly selected to be studied. This way, 15 metastable pits were totally studied for each solution. It is noted that in order to avoid any inconsistency and to obtain reliable results, those current transients which belonged to overlapping metastable pits were ignored and only single metastable pits (like the one shown in Figure 6) were studied.

Figure 9 aims to show how the kinetic parameters were assessed for the selected metastable pits. It shows *I-t* curves of two moderate metastable pits which have been typically selected from the studied pits in 0.2 M solutions of NaCl and NaBr. As seen, time and current of the pit are both regarded as zero at the initiation point.[26] As shown in the figure, in order to assess the parameters, $\log I \sim \log t$ and $\log a \sim \log t$ behaviors of the metastable pits were plotted and the linear fitting was used. For both behaviors, linear fitting was employed from the initiation point to the peak one. The fitted relationships for these typically selected pits have been included in the figure.

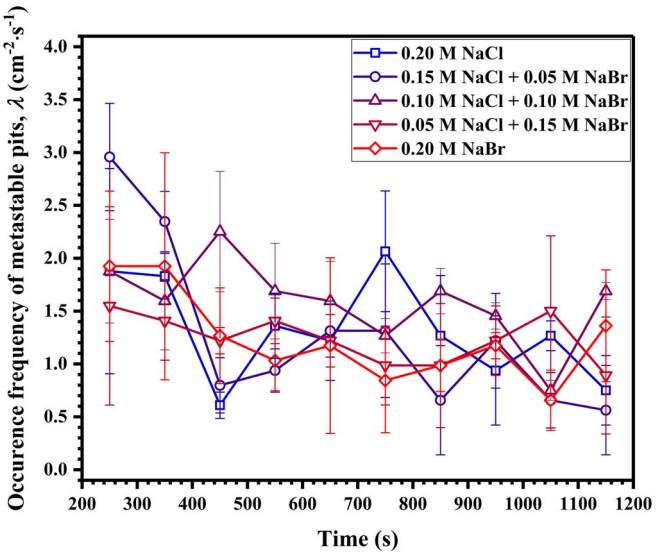

Figure 8. Comparison of the occurrence frequency of metastable pits for combined NaCl and NaBr solutions. Error bars are also representing the values of standard error obtained from 3 identical PS experiments.

Table III represents the average values of the slopes assessed for 0.2 M solutions of NaCl and NaBr. Note that based on the parameters used in Equations 6 and 7, n_I and n_a denote the slopes of the fitted lines for $\log I \sim \log t$ and $\log a \sim \log t$ behaviors, respectively; k_I and k_a also denote their corresponding intercepts. Shown values were calculated by considering the total 15 metastable pits studied in the case of each solution. As seen, both n_I and n_a are averagely lower in the case of NaBr. The intercepts of the lines are also lower when the solution bears Br^-.

Assessment of the above-defined kinetic parameters by considering several metastable pits might seem unreliable, since the number of metastable pits that appeared in PS curves is much higher. On the other hand, it is almost impractical to include all the metastable pits in evaluation of the kinetic parameters using the above-mentioned method. Hence, in order to find an alternative way to include all the metastable pits in determination of the kinetic parameters of their growth, it was attempted to use the values of peak current, radius, and growth time, which had been already calculated. To this end, the values of $\log I_{peak}$ (Figure 7a) were plotted versus the values of $\log t_g$ (Note Figure 6). The result is shown in Figure 10. Every single point on this figure is representative of an individual metastable pit which its peak current, I_{peak}, and growth time, t_g, were taken into account in statistical characterization of metastable pits. Since all the metastable pits nucleated in a given solution must more or less follow a specific growth pattern, the points in Figure 10 ought to situate around a line, the characteristics of which could be considered as the kinetic parameters of metastable pits growth. Considering the linear pattern of the points in Figure 10, this expectation seems to be true. The characteristics of the lines were obtained using linear fitting. To discriminate these characteristics from n_I and k_I, which were described earlier, they are respectively denoted N_I and K_I. As can be seen in the figure, increasing the relative concentration of the bromide in the solution reduces the values of N_I, so that its values in pure solutions of NaCl and NaBr are 0.98 and 0.55, respectively. The values of N_I for combined solutions are placed between the foregoing two. For instance, the exponent N_I for 50–50 combined solution is 0.76. K_I has also lower values in bromide bearing solutions.

In Figure 11, the values of $\log a$ (Figure 7b) were plotted versus the values of $\log t_g$. As can be seen, in this case also the points follow a linear pattern. Characteristics of the lines have been included in the figure, too. The slopes and intercepts of the lines in this figure are denoted N_a and K_a, respectively. As is evident, increment of the relative concentration of bromide in the solutions, causes the values of N_a to decrease. For the pure solution of NaCl, N_a is 0.60, whilst it is 0.47 in the case of 0.2 M solution of NaBr. For the 50–50 combined solution it is about 0.54. K_a has also a lower value when bromide is present in the solutions. The average values of N_I, K_I, N_a, and K_a for pure 0.2 M solutions of NaCl and NaBr have been included in Table III.

Figure 12 depicts typical potentiodynamic behaviors of 316 SS pencil electrodes in simulated pit solutions: 5 M HCl + 1 M NaCl and 5 M HBr + 1 M HBr. It is seen that corrosion potential, E_{corr}, could be approximately 100 mV higher in the bromide bearing pit-like solution relative to the chloride bearing one. According to the figure, by polarising the pencil electrode of 316 SS, it undergoes a rapid dissolution in both chloride and bromide bearing pit-like solutions. The rate by which the alloy is actively dissolving, $i_{diss,max}$, could be compared for chloride and bromide bearing solutions, as well. As observed, at a

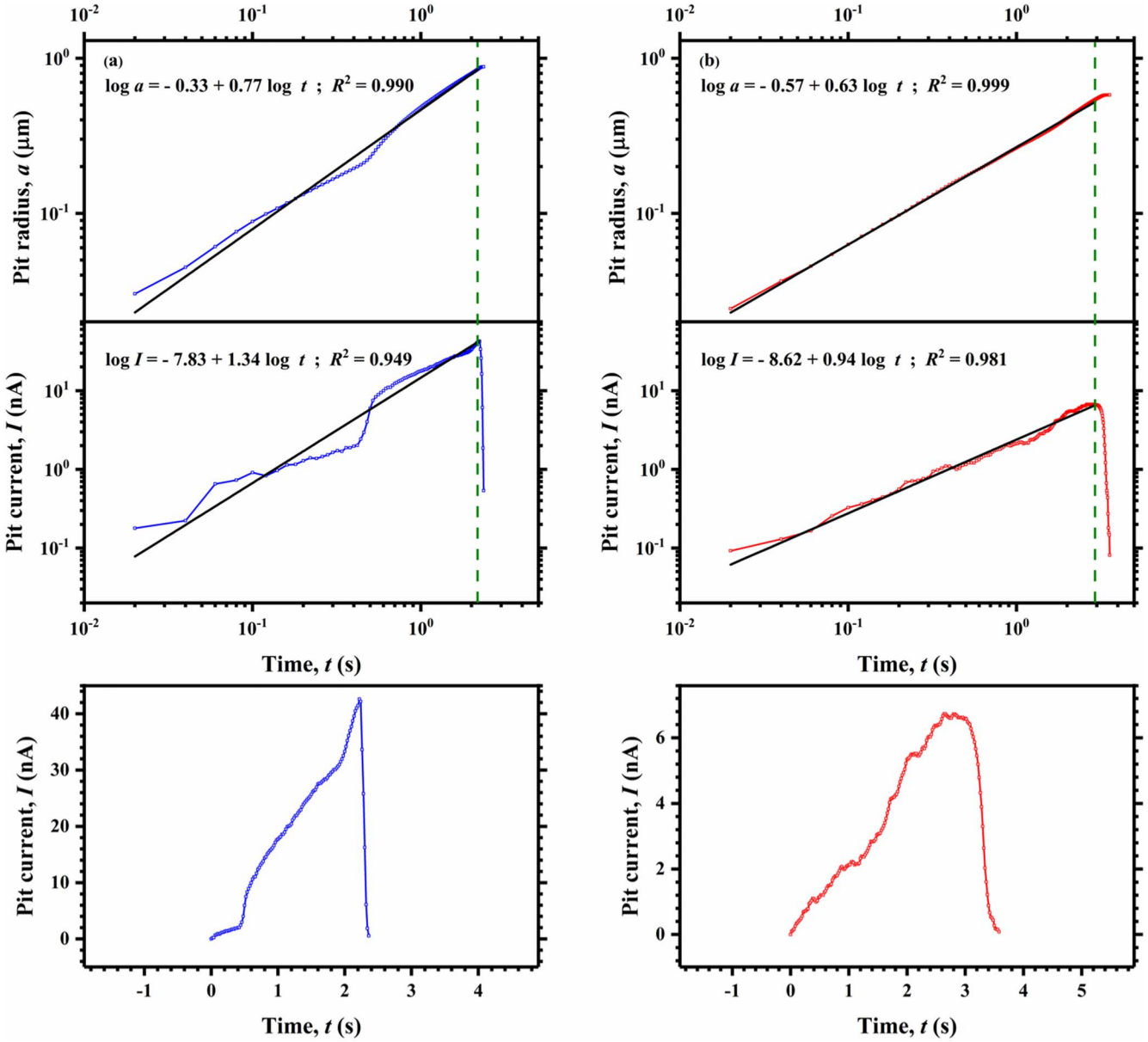

Figure 9. Two typical moderate metastable pits in a) 0.2 M NaCl and b) 0.2 M NaBr solutions with some of their respective definable quantities: lifetime, growth time, repassivation time, peak current, dissolved charge and baseline current.

Table III. The kinetic parameters of the metastable pits growth which were evaluated for 0.2 M solutions of NaCl and NaBr through different ways. Where applicable, data are represented as the mean ± standard error. The values of R^2 have been also included to indicate how close the data were to the fitted regression lines.

	0.20 M NaCl		0.20 M NaBr	
Solution	Average	R^2	Average	R^2
n_I	1.24 ± 0.05	0.957 ± 0.013	0.97 ± 0.07	0.876 ± 0.023
k_I	−7.78 ± 0.08		−8.46 ± 0.07	
n_a	0.74 ± 0.02	0.993 ± 0.002	0.64 ± 0.02	0.986 ± 0.004
k_a	−0.30 ± 0.03		−0.52 ± 0.02	
N_I	0.98 ± 0.03	0.798	0.55 ± 0.03	0.576
K_I	−7.66 ± 0.03		−8.20 ± 0.02	
N_a	0.60 ± 0.01	0.891	0.47 ± 0.01	0.852
K_a	−0.24 ± 0.01		−0.38 ± 0.01	

given applied potential, current density of the active dissolution is significantly lower in the case of 5 M HBr + 1 M NaBr solution. In other words, a given $i_{diss,max}$ is obtained at higher potentials in the case of bromide bearing pit-like solution. For instance, the potential at which the typical active dissolution current density of 1000 mA · cm^{-2} is obtained, E_{1000}, is higher in 5 M HBr + 1 M NaBr solution. In addition, it is perceived that the alloy's active dissolution is then limited by precipitation of salt and establishment of a diffusion-controlled regime, the fact which is well-known in pitting studies.[7,18,54,55] In practice, however, a supersaturation is required prior to salt precipitation.[18] Accordingly, as seen in Figure 12, salt precipitation begins at a point potential and current density of which could be respectively regarded as supersaturation potential, E_{sup}, and supersaturation current density, i_{sup}. As shown, both of E_{sup} and i_{sup} are typically higher in the case of 5 M HBr + 1 M NaBr solution. After the salt precipitation, the dissolution proceeds at a diffusion-limited current density, i_{lim}. Such tests were repeated 5 times, at least, and all of the foregoing differences for chloride and bromide bearing solutions were found to be quite

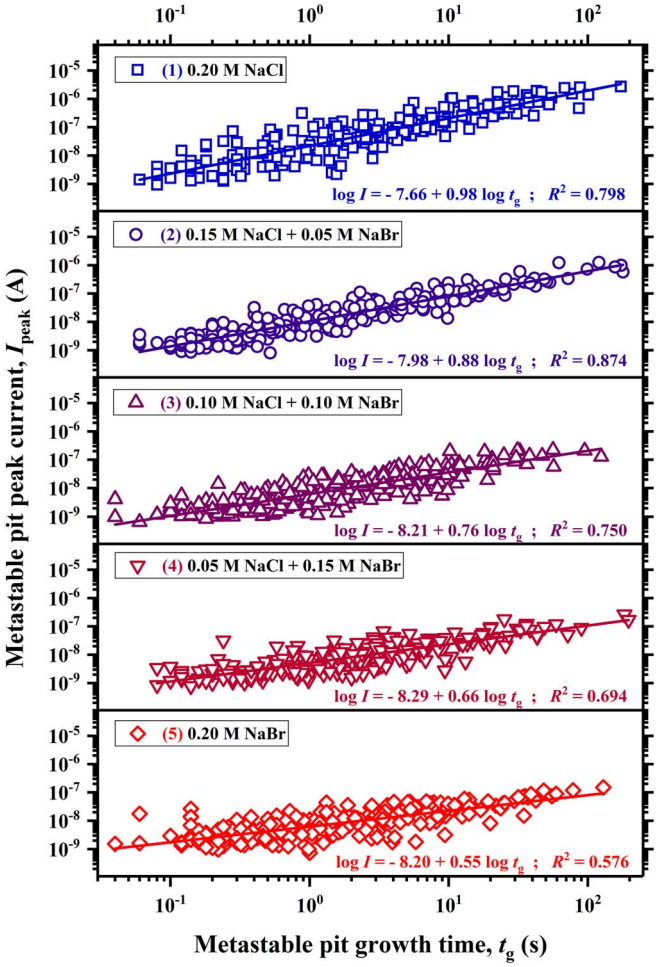

Figure 10. The linear relationship between the logarithms of metastable pit peak current, log I_{peak}, and the logarithms of metastable pit growth time, log t_g. The slope of the fitted line can be regarded as an overall estimation of the exponent N_I in the proposed kinetic relationship: $I \sim t^n$. The values for each solution have been represented in the figure.

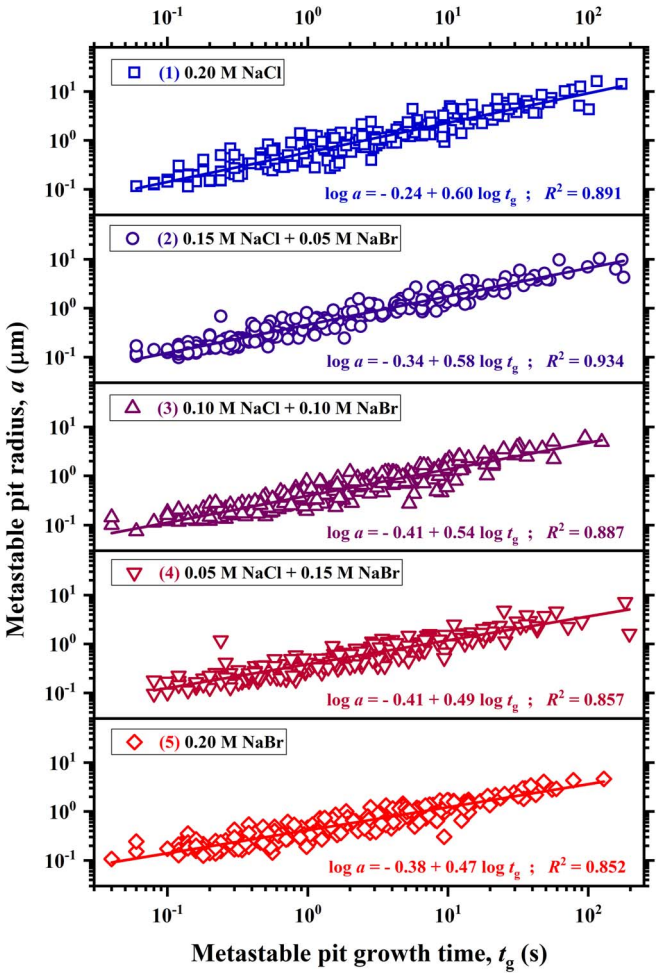

Figure 11. The linear relationship between the logarithms of metastable pit radius, log a, and the logarithms of metastable pit growth time, log t_g. The slope of the fitted line can be regarded as an overall estimation of the exponent N_a in the proposed kinetic relationship: $a \sim t^n$. The values for each solution have been represented in the figure.

reproducible. The average values of E_{corr}, E_{1000}, $i_{diss,max}$, E_{sup}, and i_{sup} are compared in Table IV. It is noted that $i_{diss,max}$ varies at different potentials; therefore, it has been compared at the typical potential of -175 mV_{SCE}.

It is noteworthy to add that in the experiments shown in Figure 12, the diffusion is not 1D and can change over the time. Thus, the values of current density in these tests might have been affected by the non-1D diffusion. Besides, the real pit solutions could be slightly different from the simulated ones, i.e. 5 M HCl + 1 M NaCl and 5 M HBr + 1 M NaBr. To address these problems and to make sure that the results shown in Figure 12 are reliable, it was attempted to acquire the values of 316 SS active dissolution rate using an alternative procedure, the results of which are represented in Figure 13. The figure aims to compare the active dissolution current density of 316 SS in NaCl and NaBr solutions in actual pit solutions. These curves belong to 1D artificial pits created using pencil electrodes. Using Faraday's law, the depths of these two artificial pits were calculated as ~350 μm. As depicted in the figure, two regions of diffusion-controlled (the region where the current density is constant due to presence of the salt layer) and activation/ohmic controlled (the region where the current density obeys a linear behavior) dissolution are obvious. According to Figure 13a, it can be said that at a given potential, the rate of alloy dissolution in the activation/ohmic controlled region is lower when the pit solution bears bromide. However, it is necessary to consider the effect of *IR* drop of the solution on the active dissolution rate

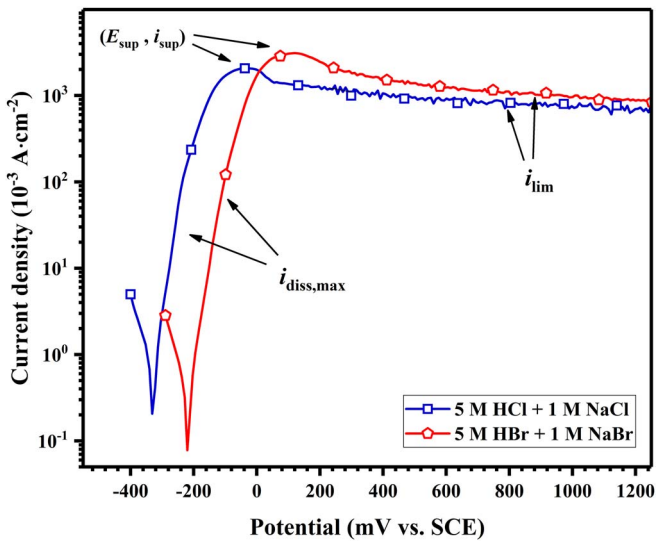

Figure 12. Typical behaviors of 316 SS pencil electrodes in simulated pit solutions: 5 M HCl + 1 M NaCl and 5 M HBr + 1 M NaBr. $i_{diss,max}$, i_{lim}, E_{sup}, and i_{sup} have been shown in the figure for both pit-like solutions.

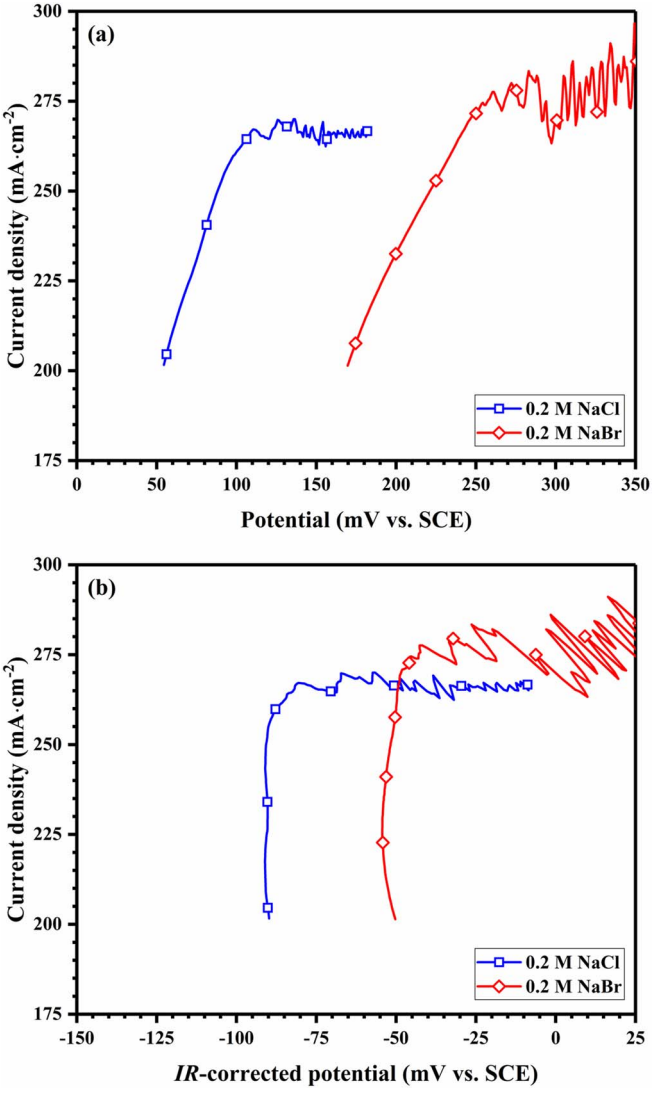

Figure 13. Comparison of the rate of alloy dissolution, $i_{diss,max}$, obtained using pencil electrodes in NaCl and NaBr solutions: a) without *IR* correction, b) with *IR* correction.

of the 316 SS. In Figure 13b, the current density is plotted versus the *IR*-corrected potentials. The values of *IR* drop in the two studied solutions were calculated from the multiplication of reciprocal slope of *i-E* curve in the activation/ohmic controlled region by the current density, according to the idea described by Laycock and Newman.[30] Comparison of the *IR*-corrected curves also indicates that the active dissolution rate of the 316 SS in the bromide bearing pit anolyte is lower than that in the chloride bearing one. The experiments were repeated several times at comparable pit depths (~350 μm) and the behaviors were found reproducible.

Discussion

The capability of Cl^- and Br^- to create an acidic environment within the pit must be taken into consideration for primary comparison of these two aggressive anions. The values of $pK_{a,eq}$ for hydrochloric and hydrobromic acids are −7 and −9, respectively.[56] These values show that in high potentials (above E_{pit}), Cl^- and Br^- are both capable of acidifying the pit solution and hampering the passivation sustainability. In other words, neither chloride nor bromide consume the protons which are produced within the cavity due to their high dissociation equilibrium constants, $K_{a,eq}$; note Equations 6 and 7:

$$HCl = H^+ + Cl^- \quad K_{a,eq} = 10^7 \qquad [6]$$

$$HBr = H^+ + Br^- \quad K_{a,eq} = 10^9 \qquad [7]$$

Effect of bromide and chloride anions on metastable pitting characteristics.—Table III lists the average values of n_I, n_a, N_I, and N_a for pure 0.2 M solutions of NaCl and NaBr, which have been calculated from different kinetic models of the metastable pits' growth. As is evident, the values of the coefficient of determination, R^2, are higher when the fitting is employed on the radius-time relationships. In other words, when the kinetic parameters of the metastable pits' growth are evaluated using the linear relationship between $\log a \sim \log t$ (Figure 9b or Figure 11), the data will be much closer to the fitted regression lines. This matter suggests that the use of radius-time relationship is more proper in describing the metastable pits growth rate. Based on this finding, thus, it is recommended to use this relationship in forthcoming works for evaluating the growth kinetics of metastable pits.

As observed, the values of N_I and N_a for both solutions are different compared to those of n_I and n_a. The reason probably returns to the overlapping metastable pits which have been taken into account in the calculation of N_I and N_a. This aside, comparison of the kinetic parameters in Table III, which were obtained through the above-mentioned different methods (illustrated by Figures 9, 10, and 11), reveals that the results are consistent and the values of n_I, n_a, N_I, and N_a are all lower in the case of NaBr solution. These lower values imply that the growth rates of metastable pits are lower in the case of bromide bearing solution.

It was figured out that the metastable pits formed in pure solution of NaCl have much greater peak currents (I_{peak}) and radii (a) in comparison with pure solution of NaBr (Figure 7 and Table II). These findings are in agreement with earlier studies conducted on 403 SS[35] and Fe-13Cr martensitic SS.[37] Considering that the median value of lifetime of metastable pits was measured to be approximately equal in both solutions, the greater values of I_{peak} and a in chloride bearing solutions can be attributed to the fact that Cl^- can promote more alloy dissolution within a metastable pit, under similar conditions. Study of the metastable pits' growth kinetics (Figures 9, 10, and 11, and Table III) substantiated this finding. The value of the exponent in $I \sim t^n$ / $a \sim t^n$ behaviors (n_I, n_a, N_I, and N_a shown in Table III) in growing metastable pits was found to be lower in the case of NaBr solutions. The lower growth/dissolution rate of metastable pits in bromide bearing solutions are in agreement with the results of pencil electrode experiments. Using pencil electrodes, it was perceived that at a given potential, the active dissolution rate of 316 SS is much lower in bromide bearing solutions compared to chloride bearing ones (Figures 12 and 13, and Table IV). Therefore, it can be deduced that those metastable pits, which grew on the 316 SS's surface in bromide solutions, have had lower values of I_{peak} and a relative to those grew in chloride solutions, due to the lower rate of alloy's active dissolution in presence of bromide.

Despite the difference in growth kinetics of metastable pits, it was found that metastable pits occurrence frequency, λ, of 316 SS in NaCl

Table IV. Average values of the key characteristics shown in Figure 12. Data are represented as the mean ± standard error.

Solution	E_{corr} (mV_{SCE})	E_{sup} (mV_{SCE})	i_{sup} ($mA \cdot cm^{-2}$)	$i_{diss,max}$ at −175 mV_{SCE} ($mA \cdot cm^{-2}$)	E_{1000} (mV_{SCE})
5 M HCl + 1 M NaCl	−326 ± 4	−33 ± 5	2689 ± 160	661 ± 55	−157 ± 4
5 M HBr + 1 M NaBr	−223 ± 4	108 ± 5	2826 ± 354	3 ± 1	−23 ± 4

and NaBr solutions is comparable (Figure 8). However, our previous study on 403 SS showed a higher λ in NaCl solutions compared to NaBr ones.[35] This inconsistency might be due to the higher content of alloyed Mo in 316 SS compared to 403 SS. Alloyed Mo could reduce the number of pit nucleation/metastable pitting events on SS.[24] On the other hand, it is reported that alloyed Mo provides much more extra resistance to pitting corrosion in chloride solutions than in bromide ones.[57] Thus, comparable values of λ for 316 SS in NaCl and NaBr solutions seems to be due to the more extra resistance to pitting nucleation/metastable pitting which is attained by alloyed Mo.

Effect of bromide and chloride anions on pitting potential of 316 SS.—The fact that the metastable pits which nucleated in NaBr solution have lower values of stability product compared to those nucleated in NaCl one (Figure 7 and Table III), suggests that they are more probable to repassivate. On the assumption that the critical stability product required for the pit stabilization is comparable in both NaCl and NaBr solutions (these critical values will be discussed in the article's part II), lower values of metastable pits' stability product in bromide bearing solutions can imply that they need more intense conditions for transition to stability. It is, therefore, in line with the results of pitting potential, E_{pit} (Figures 2 and 3). Since the pits nucleated in the presence of bromide require more intense circumstances to become stable, their stability must happen at higher potentials. Comparison of this quantity for different solutions (Figures 2 and 3) indicates that the pitting corrosion of 316 SS is actually more probable in chloride bearing solutions. Besides, E_{pit} of 316 SS, rises by increasing the relative concentration of bromide in the solution. This observation had been also reported previously[31] and it is consistent with the aforesaid order of aggressivity: $Cl^- > Br^-$.

The higher E_{pit} in the case of bromide bearing solutions could be explained by considering the rate of alloy's active dissolution in pit-like solution, as well. Recently, a unifying set of criteria for pit stabilization has been elaborated by Li et al.[18] According to them, for an open pit to be stabilized, the maximum rate of alloy dissolution at the pit surface, $i_{diss,max}$, must sufficiently exceed a critical current density, $i_{diff,crit}$, which is required for maintaining the critical concentration of alloy's cations at the pit surface, C_{crit}. Otherwise, the pit anolyte is diluted and the pit surface is repassivated. For salt precipitation, on the other hand, $i_{diss,max}$ must exceed the diffusion-limited current density, i_{lim}, which is associated with attainment of the saturation concentration of cations at the pit surface, C_{sat}. Taking these elucidations into account and considering the results shown in Figures 12 and 13, and Table IV, it can be deduced that a predominant factor retarding the pit transition from metastability to stability in presence of bromide should be hindrance of alloy's dissolution, $i_{diss,max}$ (Figures 12 and 13). The inhibitory effect of bromide on anodic dissolution has been similarly reported by others, too.[31,39,57] Hence, decrement of $i_{diss,max}$ could explain why E_{pit} of 316 SS in bromide bearing media is higher relative to the chloride bearing ones (Figures 2 and 3). It could also clarify why its repassivation potential, E_{rep}, have higher values in the case of NaBr solutions (Figure 4). Since active dissolution rate in the case of bromide bearing solution is lower, the criterion $i_{diss,max} \leq i_{diff,crit}$ for pit repassivation could be satisfied at higher potentials.

It is noted that there should be other factors contributing to retardation of the pitting stabilization in bromide bearing media besides decrement of $i_{diss,max}$, such as increment of i_{lim}, increment of $i_{diff,crit}$, increment of the ohmic resistance of the solution exists within the pit, and reduction in the occlusion of pit lacy cover.[18,30,58] Detailed study of the contribution of these factors will be addressed in a subsequent publication.

Although it has been reported that when ~5% Mo exists in the SS's composition, chloride aggressivity is lower than bromide,[38,39] results of 316 SS showed the higher aggressivity for chloride similar to other low Mo or Mo-free SSs.[31–37] This implies that a minimum threshold of Mo content is required to alter the aggressivity order of chloride and bromide.

Conclusions

According to the results obtained in this work, which deals with the metastable and stable pitting of 316 austenitic SS in chloride and bromide bearing solutions, the following phrases can be stated, as conclusions:

1. The aggressivity of chloride for 316 austenitic stainless steel is more than that of bromide. Pitting potentials are much lower in chloride bearing solutions compared to the bromide bearing ones. The slope of the $E_{pit} - \log C_{agg}$ for chloride is higher than that for bromide.
2. The repassivation potential of flat electrodes, E_{rep}, increases by increment of the Br^-:Cl^- concentration ratio. The highest E_{rep} is hence 134 mV_{SCE} and belongs to the pure NaBr solution. The lowest E_{rep} has been also obtained for pure NaCl one and it equals to 34 mV_{SCE}.
3. The occurrence frequency of metastable pits were comparable in NaCl and NaBr solutions. However, the values of metastable pits peak current, I_{peak} and radius, a decrease by decreasing the relative concentration of bromide in the solution. Besides, the highest value of stability product, $i \cdot a$, was obtained in pure NaCl solution. The median values of metastable pits stability product for pure NaCl and NaBr solutions are 8.834 and 2.629 $mA \cdot m^{-1}$, respectively.
4. Increasing the relative concentration of Br- in the environment reduces the growth kinetics of metastable pits. The value of the exponent in $I \sim t^n$ / $a \sim t^n$ behaviors of metastably growing pits is lower in solutions with higher concentration of bromide.
5. Hindrance of the 316 SS active dissolution in presence of bromide seems to be a rationale behind the reduced growth kinetics of metastable pits and increased pitting/repassivation potentials in NaBr solutions. At the typical of −175 mV_{SCE}, the maximum current density by which pencil electrode of 316 SS actively dissolves in contact with the bromide-free pit-like solution of 5 M HCl + 1 M NaCl is almost 661 $mA \cdot cm^{-2}$. In presence of bromide, i.e. in 5 M HBr + 1 M NaBr solution, it can be reduced to averagely 3 $mA \cdot cm^{-2}$, though.

Acknowledgments

Authors thank the Iran Ferdowsi University of Mashhad, due to financial supports (sponsorship No. 3/32773) and providing equipment required in corrosion research. Prof. G.S. Frankel is also highly acknowledged due to his constructive suggestions.

ORCID

S. Pahlavan https://orcid.org/0000-0002-2207-9691
M. H. Moayed https://orcid.org/0000-0002-4296-8496

References

1. J. R. Davis, *Stainless steels*, p. 577, ASM International, (1994).
2. A. J. Sedriks, (1996).
3. M. G. Alvarez and J. R. Galvele, *Shreir's Corrosion*, p. 772, Elsevier, (2010).
4. G. S. Frankel, *J. Electrochem. Soc.*, **145**, 2186 (1998).
5. E. McCafferty, *Introduction to Corrosion Science*, p. 302, Springer Science & Business Media, (2010).
6. P. C. Pistorius and G. T. Burstein, *Philos. Trans. R. Soc. A: Math. Phys. Eng. Sci.*, **341**, 531 (1992).
7. J. Soltis, *Corros. Sci.*, **90**, 5 (2015).
8. G. Bai, S. Lu, D. Li, and Y. Li, *Corros. Sci.*, **108**, 111 (2016).
9. A. Abbasi Aghuy, M. Zakeri, M. H. Moayed, and M. Mazinani, *Corros. Sci.*, **94**, 368 (2015).
10. T. Li, J. R. Scully, and G. S. Frankel, *J. Electrochem. Soc.*, **165**, C484 (2018).
11. G. S. Frankel, L. Stockert, F. Hunkeler, and H. Boehni, *Corrosion*, **43**, 429 (1987).
12. P. Ernst, N. J. Laycock, M. H. Moayed, and R. C. Newman, *Corros. Sci.*, **39**, 1133 (1997).
13. P. Ernst and R. Newman, *Corros. Sci.*, **44**, 927 (2002).
14. L. Garfias-Mesias and J. Sykes, *Corros. Sci.*, **41**, 959 (1999).
15. S. Heurtault, R. Robin, F. Rouillard, and V. Vivier, *Electrochim. Acta*, **203**, 316 (2016).

16. M. Ghahari et al., *Corros. Sci.*, **100**, 23 (2015).
17. T. Li, L. Liu, B. Zhang, Y. Li, and F. Wang, *Corros. Sci.*, **124**, 46 (2017).
18. T. Li, J. R. Scully, and G. S. Frankel, *J. Electrochem. Soc.*, **165**, C762 (2018).
19. P. C. Pistorius and G. T. Burstein, *Corros. Sci.*, **33**, 1885 (1992).
20. G. S. Frankel, L. Stockert, F. Hunkeler, and H. Boehni, *Corrosion*, **43**, 7 (1987).
21. P. C. Pistorius and G. T. Burstein, *Corros. Sci.*, **36**, 525 (1994).
22. D. Nakhaie and M. H. Moayed, *Corros. Sci.*, **80**, 290 (2014).
23. S. Al Saadi, Y. Yi, P. Cho, C. Jang, and P. Beeley, *Corros. Sci.*, **111**, 720 (2016).
24. G. O. Ilevbare and G. T. Burstein, *Corros. Sci.*, **43**, 485 (2001).
25. Y. Tang et al., *Corros. Sci.*, **80**, 111 (2014).
26. M. H. Moayed and R. C. Newman, *Corros. Sci.*, **48**, 1004 (2006).
27. J. R. Galvele, *J. Electrochem. Soc.*, **123**, 464 (1976).
28. J. Galvele, *Corros. Sci.*, **21**, 551 (1981).
29. T. Rayment et al., *Electrochem. commun.*, **10**, 855 (2008).
30. N. J. Laycock and R. C. Newman, *Corros. Sci.*, **39**, 1771 (1997).
31. M. Kaneko and H. S. Isaacs, *Corros. Sci.*, **42**, 67 (2000).
32. M. Janik-Czachor, *Mater. Corros. und Korrosion*, **30**, 255 (1979).
33. C. M. A. Brett and P. I. C. Melo, *J. Appl. Electrochem.*, **27**, 959 (1997).
34. S. U. Lee, J. C. Ahn, D. H. Kim, S. C. Hong, and K. S. Lee, *Mater. Sci. Eng. A*, **434**, 155 (2006).
35. S. Pahlavan et al., *Corros. Sci.*, **112**, 233 (2016).
36. S. A. M. Refaey, F. Taha, and A. M. A. El-Malak, *Appl. Surf. Sci.*, **242**, 114 (2005).
37. D. D. Macdonald and X. Lei, *J. Electrochem. Soc.*, **163**, C738 (2016).
38. E. A. Abd El Meguid, *Corrosion*, **53**, 623 (1997).
39. M. Kaneko and H. S. Isaacs, *Corros. Sci.*, **44**, 1825 (2002).
40. P. Lu, G. R. Engelhardt, B. Kursten, and D. D. Macdonald, *J. Electrochem. Soc.*, **163**, C156 (2016).
41. D. Nakhaie, M. Zakeri, M. Naghizadeh, and M. H. Moayed, *J. Electrochem. Soc.*, **162**, C121 (2015).
42. X. Feng, X. Lu, Y. Zuo, N. Zhuang, and D. Chen, *Corros. Sci.*, **103**, 223 (2016).
43. E. O. Nunez Moran, *thesis*, The Ohio State University (2010).
44. P. Ernst and R. C. Newman, *Corros. Sci.*, **44**, 943 (2002).
45. M. Gholami, M. Hoseinpoor, and M. H. Moayed, *Corros. Sci.*, **94**, 156 (2015).
46. T. Shibata, *Corrosion*, **52**, 813 (1996).
47. T. Shibata and T. Takeyama, *Corrosion*, **33**, 243 (1977).
48. J. R. Galvele and S. M. de De Micheli, *Corros. Sci.*, **10**, 795 (1970).
49. R. C. Newman, M. A. A. Ajjawi, H. Ezuber, and S. Turgoose, *Corros. Sci.*, **28**, 471 (1988).
50. W. Tian, N. Du, S. Li, S. Chen, and Q. Wu, *Corros. Sci.*, **85**, 372 (2014).
51. L. Guan, Y. Zhou, B. Zhang, J. Q. Wang, E.-H. Han, and W. Ke, *Int. J. Electrochem. Sci.*, **11** (2016).
52. Rs. Lillard, G. Vasquez Jr, and D. F. Bahr, *Corrosion*, **66**, 75004 (2010).
53. Y. Wang, G. Wu, L. He, and P. M. Singh, *Corrosion*, **72**, 628 (2016).
54. R. C. Newman and M. A. A. Ajjawi, *Corros. Sci.*, **26**, 1057 (1986).
55. M. Naghizadeh, D. Nakhaie, M. Zakeri, and M. H. Moayed, *J. Electrochem. Soc.*, **162**, C71 (2014).
56. R. P. Bell, *The Proton in Chemistry*, p. 91, Springer US, Boston, MA, (1973).
57. P. Ernst and R. C. Newman, *Electrochem. Solid-State Lett.*, **11**, C1 (2008).
58. M. Zakeri, M. Naghizadeh, D. Nakhaie, and M. H. Moayed, *J. Electrochem. Soc.*, **163**, C275 (2016).